JOURNAL OF THERMOPHYSICS AND HEAT TRANSFER
Vol. 9, No. 1, January–March 1995

Computation of Nonequilibrium Radiating Shock Layers

Tahir Gökçen*
Eloret Institute, Palo Alto, California 94303

A computational technique of coupling radiative transfer to fluid motion is developed for axisymmetric blunt body shock layer flows in a thermochemical nonequilibrium environment. The coupled formulation of radiation and flowfield leads to a governing set of integro-differential equations. This equation set is solved using a modified Gauss-Seidel line relaxation technique that incorporates the inversion of full block matrix associated with radiative transfer using a block iteration method. The thermodynamic state of the gas is described by three temperatures: 1) translational, 2) rotational, and 3) vibrational-electronic. Radiation phenomenon is assumed to be governed by the vibrational-electronic temperature. The radiative properties are described by a spectrally detailed model. The computations are presented for two cases, including the Fire II flight experiment. It is shown that the method converges and the calculated spectra qualitatively agree with the experimental data for the two test cases. The calculated total radiative flux underestimates the measured values owing to the low vibrational-electronic temperature predicted in the flowfield calculation.

Nomenclature

B_λ = Planck function at wavelength λ
E = total energy per unit volume
E_r = total rotational energy per unit volume
E_v = total vibrational energy per unit volume
$\boldsymbol{F}$ = x component of convective flux vector
$\boldsymbol{F}_R$ = flux vector for radiation
$\boldsymbol{G}$ = y component of convective flux vector
$\boldsymbol{H}$ = source vector for axisymmetric geometry
h_0 = total enthalpy
I_λ = intensity of radiation at wavelength λ
M_i = molecular weight of species i
p = pressure
q_R = total radiative heat flux
q_λ = spectral radiative flux at wavelength λ
q_λ^+ = spectral radiative flux in $+s$ direction
q_λ^- = spectral radiative flux in $-s$ direction
s = coordinate for tangent-slab approximation
T = translational temperature
T_r = rotational temperature
T_v = vibrational-electronic temperature
$\boldsymbol{U}$ = state vector
u = x component of velocity
v = y component of velocity
$\boldsymbol{W}$ = source vector for thermochemistry
w_i = source term in species equation i
w_r = source term in rotational energy equation
w_v = source term in vibrational energy equation
ε_n = exponential integral function of order n
κ_λ = absorption coefficient at wavelength λ
λ = wavelength
ρ = density
ρ_i = density of species i
σ_λ^i = absorption cross section of species i at λ
τ_λ = optical thickness at wavelength λ

Presented as Paper 93-0144 at the AIAA 31st Aerospace Sciences Meeting, Reno, NV, Jan. 10–13, 1993; received March 14, 1994; revision received July 18, 1994; accepted for publication Aug. 16, 1994.

*Research Scientist, 3788 Fabian Way; currently at NASA Ames Research Center, M/S 230-2, Moffett Field, CA 94035. Member AIAA.

Introduction

WHEN a space vehicle enters into the Earth's atmosphere from space, the temperature in the shock layer formed over the vehicle may become so high that the gas radiates. The radiative energy transfer to the surface of the vehicle then becomes an important engineering consideration. Prediction of radiative heat transfer rates to re-entry vehicles and the problem of coupling between radiation and flowfield for chemically reacting flows have been of interest to a number of researchers.[1–10]

For realistic calculations of radiative heat transfer, several requirements must be satisfied. The flowfield thermochemistry must be predicted accurately because nonequilibrium processes such as vibrational relaxation and ionization have dominant effects on radiation. The radiation transport model must include the effect of emission and absorption with a detailed spectral variation. Finally, special care must be given to the coupling between flowfield and radiation.

For some aerothermodynamic flow problems, the effects of emission and absorption on flowfield can be neglected, and the radiative energy flux to the wall can be calculated from the nonradiating flowfield solution. That is, the radiation and flowfield are uncoupled, and the radiative transfer and flowfield analyses are carried out separately. On the other hand, for problems such as predicting aerobrake flow environments of planetary entry vehicles, radiative transfer becomes significant enough that its presence can alter the flowfield, which in turn affects the radiative heat flux at the wall. That is, the radiation and flowfield are coupled, and therefore, a simultaneous treatment of radiation and flowfield is necessary. This coupling leads to a set of integro-differential equations that are much more complicated than the governing differential equations for the uncoupled flows.

Researchers have presented several approaches for the analyses of radiating shock layers. These analyses differ from each other in radiative transport models used and in the degrees of coupling between radiation and flowfield.

The objective of this article is to present a new numerical approach to solve fully coupled equations of flowfield and radiation using an implicit modified Gauss-Seidel line relaxation method. The method is applied to the axisymmetric, thermochemical nonequilibrium shock layer flows. The calculations are carried out for two test cases for which experimental data exist: 1) a hypothetical blunt body flow with the same flow conditions as in the shock-tube experiment,[11,12] and 2) the Fire II flight experiment.[13–15]

Formulation

The present nonequilibrium gas model for air consists of 11 chemical species. The thermal state of the gas is described by three temperatures: 1) translational, 2) rotational, and 3) vibrational-electronic. The radiative energy transport is assumed to be one-dimensional, the dimension being normal to the wall. This is the so-called tangent-slab approximation that is applicable to the stagnation region of a blunt body or to blunt bodies of which radius of curvature is much larger than the shock layer thickness. In radiative transfer calculations, gases are assumed to be nongray, absorbing, and emitting with a detailed spectral dependency of the absorption coefficient. The flow is assumed to be inviscid. The viscous boundary layer is neglected for the purpose of radiative transfer calculation.[16,17] Based on the work of Whiting and Park,[16] the self-absorption of atomic lines behind the shock are so strong that neglecting absorption in the boundary layer may be justified.

The governing Euler equations are augmented with the equations accounting for thermochemical nonequilibrium processes. The equation set consists of 16 partial differential equations: 11 mass conservation equations for species, 2 momentum equations for two-dimensional flows, and 3 energy equations.

Governing Equations

The governing Euler equations for nonequilibrium air have been described in detail elsewhere.[18,19] For two-dimensional/axisymmetric inviscid flows, the equation set in Cartesian coordinates can be written in conservation form of

$$\frac{\partial U}{\partial t} + \frac{\partial F}{\partial x} + \frac{1}{y^r}\frac{\partial}{\partial y} y^r G + \frac{\partial F_R}{\partial s} = W + \frac{rH}{y} \tag{1}$$

where $r = 1$ for axisymmetric flows, and $r = 0$ for two-dimensional flows. Components of the state vector $\boldsymbol{U}$, the convective flux vectors $\boldsymbol{F}$ and $\boldsymbol{G}$, the flux vector for radiation $\boldsymbol{F}_R$, and the source vectors $\boldsymbol{W}$ for thermochemistry and $\boldsymbol{H}$ for axisymmetric geometry in Eq. (1), are given as follows:

$$\boldsymbol{U} = \begin{bmatrix} \rho_1 \\ \rho_2 \\ \vdots \\ \rho_{11} \\ \rho u \\ \rho v \\ E_v \\ E_r \\ E \end{bmatrix}, \quad \boldsymbol{F} = \begin{bmatrix} \rho_1 u \\ \rho_2 u \\ \vdots \\ \rho_{11} u \\ \rho u^2 + p \\ \rho uv \\ uE_v \\ uE_r \\ u(E+p) \end{bmatrix}, \quad \boldsymbol{G} = \begin{bmatrix} \rho_1 v \\ \rho_2 v \\ \vdots \\ \rho_{11} v \\ \rho uv \\ \rho v^2 + p \\ vE_v \\ vE_r \\ v(E+p) \end{bmatrix} \tag{2}$$

$$\boldsymbol{F}_R = \begin{bmatrix} 0 \\ 0 \\ \vdots \\ 0 \\ 0 \\ 0 \\ q_R \\ 0 \\ q_R \end{bmatrix}, \quad \boldsymbol{W} = \begin{bmatrix} w_1 \\ w_2 \\ \vdots \\ w_{11} \\ 0 \\ 0 \\ w_v \\ w_r \\ 0 \end{bmatrix}, \quad \boldsymbol{H} = \begin{bmatrix} 0 \\ 0 \\ \vdots \\ 0 \\ 0 \\ p \\ 0 \\ 0 \\ 0 \end{bmatrix}$$

The radiative flux q_R, which appears as a heating term in the energy equations, needs to be expressed in terms of flow quantities. Therefore, Eq. (2) is supplemented by the equation of radiative transfer. Since the vibrational energy contains the electronic energy within the framework of the two-temperature model, q_R also appears in the vibrational energy equation. The source terms for thermochemical nonequilibrium processes are described in detail elsewhere,[18,19] therefore, they will not be repeated here. However, the derivation of the radiative heat flux is given below.

Thermochemistry Model

The nonequilibrium gas model for air consists of eleven chemical species (N_2, O_2, NO, N, O, N_2^+, O_2^+, NO^+, N^+, O^+, e^-), and the thermal state of the gas is described by three temperatures: 1) translational, 2) rotational, and 3) vibrational-electronic. The thermochemistry model is basically that proposed by Park.[17,18] The relaxation time for vibrational-translational energy exchange is taken from Millikan and White[20] with Park's modification, which accounts for the limiting cross section at high temperatures. The rotational relaxation times are calculated assuming a constant collision number of 5. For dissociation-vibration coupling, the average vibrational energy lost or gained due to dissociation and recombination is specified as 30% of the dissociation energy.[18] The chemical reaction rates are prescribed by Park's model where the basic dissociation rate is assumed to be governed by the geometric average of translational and vibrational temperatures.

The present thermochemistry model is tested against experimental data and a particle method.[21,22] Using a relatively fine grid, it is found that the model can satisfactorily reproduce both dissociation and vibrational-electronic temperature for dissociation dominated flows.

Radiation Transport Model

The radiative energy transport is assumed to be one dimensional, the dimension being normal to the wall. The thermal radiation is assumed to be governed by the vibrational-electronic temperature.[17] Since the radiation is mostly due to transitions from electronic states of atoms and molecules and transitions of electrons between the bound and free states, vibrational-electronic temperature is the relevant parameter. The gases are assumed to be nongray, and the spectral absorption coefficients of the species are described by 2371 absorption bands in the range $\lambda = 0.075$–1.5 μm. The number and wavelength range of absorption bands are semiempirically selected by Park.[23]

The spectral absorption coefficient of the gas is computed using

$$\kappa_\lambda = \sum_i \rho_i \sigma_\lambda^i / M_i \tag{3}$$

The curve-fits for absorption cross sections of radiating species (N_2, O_2, NO, N, O, N_2^+) are provided by Park[23] in the form

$$\ln(\sigma_\lambda^i) = A_{1\lambda}^i/z + A_{2\lambda}^i + A_{3\lambda}^i \ln(z) + A_{4\lambda}^i z + A_{5\lambda}^i z^2 \tag{4}$$

where $z = 10{,}000/T_v$. These absorption coefficient curve-fits are partially validated with the benchmark computations of NEQAIR.[24]

Although the derivation of q_R from the equation of radiative transfer can be found in a standard textbook on this subject, it is briefly outlined herein for the tangent-slab model shown in Fig. 1.

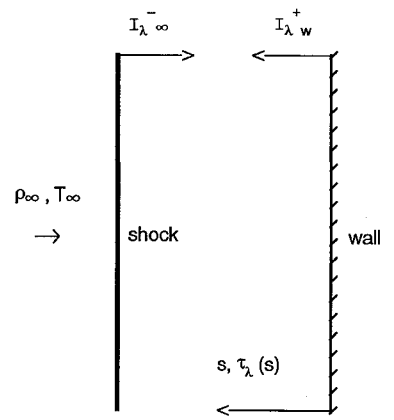

Fig. 1 Geometry of the tangent-slab model.

The intensity of radiation for a ray at λ is given by the equation of radiative transfer

$$l\frac{\partial I_\lambda}{\partial \tau_\lambda} = B_\lambda - I_\lambda \tag{5}$$

where the optical thickness is defined as

$$\tau_\lambda = \int_w^s \kappa_\lambda \, ds \tag{6}$$

and l is the direction cosine. The intensity for a given l in terms of optical thickness can be found through integration of Eq. (5)

$$I_\lambda(s, l) = I_b e^{-(\tau-\tau_b)/l} + \int_{\tau_b}^{\tau} \frac{B_\lambda}{l} e^{-(\tau-\tau')/l} \, d\tau' \tag{7}$$

where I_b denotes the boundary value of the ray.

Once the intensity of the radiation is known, the spectral flux is computed as

$$q_\lambda(\tau) = 2\pi \int_{-1}^{1} I_\lambda l \, dl \tag{8}$$

It is convenient to introduce half-range fluxes to handle boundary conditions for the intensity of radiation. Then the net spectral radiative flux is given by

$$q_\lambda = q_\lambda^+ - q_\lambda^- \tag{9}$$

After carrying out the integration in Eq. (8), the half-range fluxes can be expressed as

$$\begin{aligned} q_\lambda^+(\tau) &= 2\pi \left[I_w \varepsilon_3(\tau) + \int_{\tau_w}^{\tau} B_\lambda \varepsilon_2(\tau - \tau') \, d\tau' \right] \\ q_\lambda^-(\tau) &= 2\pi \left[I_\infty \varepsilon_3(\tau_\infty - \tau) + \int_{\tau}^{\tau_\infty} B_\lambda \varepsilon_2(\tau' - \tau) \, d\tau' \right] \end{aligned} \tag{10}$$

where I_∞ and I_w are the boundary values of the intensity, and $\varepsilon_n(\tau)$ is the exponential integral function of order n defined as

$$\varepsilon_n(\tau) = \int_0^1 l^{n-2} \exp[-(\tau/l)] \, dl \tag{11}$$

For the computations of $\varepsilon_n(\tau)$ functions, the polynomial and rational approximations are used.[25]

Finally, the total radiative flux is obtained through integration over the spectrum of interest

$$q_R = \sum_\lambda q_\lambda \Delta\lambda \tag{12}$$

Numerical Method

The numerical approach to solve the governing equations follows the previous works on nonreacting and reacting flows and incorporates several features developed earlier.[26-28] The governing equations are discretized using a finite volume approach, and the resulting difference equations are solved using a fully implicit method for fluid dynamics, chemistry, and radiative transfer. The method uses flux vector splitting for convective fluxes. Shock capturing, along with adaptive grid strategy, is also implemented. The implicit treatments of convective fluxes and source terms are given in Refs. 27 and 28, in detail. The implicit treatment of radiative flux for quasi-one-dimensional flows given in Ref. 7 results in the full block matrix difference equations. The full matrix is inverted iteratively using block iteration methods.[7]

The treatment of radiative flux and how it affects the matrix structure of difference equations is briefly outlined here. Let us consider an i line where the tangent-slab approximation is used. The implicit approximation to the radiative flux at any $j + \frac{1}{2}$ surface of i line can be written as

$$q_{Rj+1/2}^{n+1} = q_{Rj+1/2}^{n} + \sum_{k=2}^{JL} \frac{\partial q_R}{\partial U_k} \delta U_k^n \tag{13}$$

Since the second term on the right side of Eq. (13) involves the sum of all the points along the i line, the implicit finite difference equations for point j of the i line then take the form

$$\sum_{m=2}^{JL} \tilde{A}_{j,m} \delta U_m^n = \Delta U_j^n \tag{14}$$

where ΔU^n and δU^n represent the explicit and implicit approximations to the solution. The matrix $\tilde{A}_{j,m}$ has a banded structure for nonradiating flows, which is no longer true for radiating flows because of the radiative flux Jacobian. One can invert $\tilde{A}_{j,m}$ directly or use a block iterative method. For the existing Gauss-Seidel line relaxation methods block tridiagonal iteration

$$\begin{aligned} &\tilde{A}_{j,j-1}\delta U_{j-1}^{k+1} + \tilde{A}_{j,j}\delta U_j^{k+1} + \tilde{A}_{j,j+1}\delta U_{j+1}^{k+1} \\ &\quad = \Delta U_j^n - \sum_{2}^{j-2} \tilde{A}_{j,m}\delta U_m^k - \sum_{j+2}^{JL} \tilde{A}_{j,m}\delta U_m^k \end{aligned} \tag{15}$$

is of interest. The right side of Eq. (15) is added to the Gauss-Seidel terms in the existing line relaxation method used for the nonradiating flow computations.[28]

The convergence of this numerical approach relies on the premise that the implicit matrix of finite difference equations is diagonally dominant. For flows with no radiative transfer, the diagonal dominance is satisfied when an upwind differencing scheme for convective flux vectors is used. The implicit treatment of source terms adds terms to diagonal blocks such that the diagonally dominant structure is strengthened. With introduction of the radiative transfer, the resulting implicit matrix is not necessarily diagonally dominant because of the integration involved in the radiative fluxes. Although it is rather difficult to determine all the physical parameters for which the diagonal dominance is not preserved, one can expect that this occurs when radiation in the flowfield is stronger than convection phenomena. Nevertheless, for the flows considered in the present work, the diagonal dominance appears to be preserved and the modified Gauss-Seidel line relaxation method converges.

Presentation of Results

Two different axisymmetric blunt body flows with nonequilibrium thermochemistry and radiation are computed. The first is the flow over a sphere at the freestream conditions corresponding to the shock tube experiments of Allen et al.[11] and Sharma et al.[12] These experiments measured the radiation emission behind the normal shock wave.

The second is the flow over the Fire II vehicle geometry at the freestream conditions corresponding to its flight trajectory at $t = 1634.25$ s. The Fire II flight experiment was associated with the Apollo project during the 1960s. This experiment measured convective and radiative heat fluxes at various locations on the surface of an Apollo-shaped blunt body.[13,14] The spectral distribution of radiation intensity at the stagnation point was also measured by radiometers.[15]

In both computations a 50×30 adaptive grid is used. The grid is fairly coarse because of the computational limitations brought by the detailed radiation model. The convergence of coupled solution is obtained within 200 steps because of the

implicit method used. The coupled radiation calculations require between 12–15 CPU hours on a Cray Y-MP. The computing time is not scaled similarly by the number of points in both directions. The computing time scales linearly with the number of points along the body, and it is approximately proportional to the square of the number of points normal to the wall and the number of spectral points in the radiation model.

Shock Tube Case

For the shock tube case, the freestream conditions are: $u_\infty = 10$ km/s, $T_\infty = 300$ K, and $p_\infty = 0.1$ Torr.

Figure 2 shows the convergence history of total radiation flux at the stagnation point. The total radiative flux is obtained by integrating the spectral flux over the wavelength. The starting flow conditions for coupled flowfield are obtained from the converged flowfield with no radiative transfer. The difference between the initial and converged values of radiative flux represents the difference between the uncoupled and coupled flux values. The radiative flux at stagnation point is overestimated by more than a factor of 2 when it is computed from an uncoupled flowfield.

The effects of radiation coupling on stagnation streamline temperature profiles are presented in Fig. 3. Note that the radiation coupling results in lower vibrational-electronic temperature T_v near the wall due to the radiative cooling. This is expected because the radiative emission process removes energy from the vibrational-electronic mode. The radiation coupling appears to increase the nonequilibrium zone behind the shock and not affect the shock standoff distance. This increase in the nonequilibrium zone results in a slightly higher translational temperature for the coupled case, which is caused by the two-temperature modeling of thermochemistry.

It is also observed that the computed vibrational-electronic temperature behind the shock is slightly lower than the measurements of Sharma et al.[12] The computed temperature is approximately 5% lower than the experimental data at peak radiation point. The lower vibrational-electronic temperature behind the shock might have resulted from the vibrational relaxation model and/or poor resolution due to the coarse grid used in the computations. One-dimensional computations of shock wave with more refined grids (100 and 200 points) are carried out to investigate the grid sensitivity of the vibrational-electronic temperature. These computations suggest that the vibrational-electronic temperature has been computed satisfactorily near the shock with the adaptive grid used, therefore, the lower temperature values seem to result from the current vibrational relaxation model. It is known that the vibrational-electronic temperature of flowfield is very sensitive to the dissociation-vibration coupling models used.[5,22]

The computed incoming q_λ^- at the stagnation point is plotted in Fig. 4. The variation of flux in the wavelength clearly shows the nongray nature of flowfield. Note that both atomic lines and molecular bands contribute to the total value of the radiative flux. The radiation coming from the atomic lines below 0.2 μm appears to be strong.

The computed radiative loss, the divergence of spectrally integrated flux along the stagnation streamline, is shown in Fig. 5. The radiative loss is maximum immediately behind the shock. The behavior that radiative loss curve rebounds behind the shock is probably because of the increase in static enthalpy toward the wall due to deceleration of the flow.

Two sets of experimental data, AVCO experiments by Allen et al.[11] and Ames experiments by Sharma et al.,[12] in wavelength range 0.3–0.7 μm are shown in Fig. 6. The radiation measurements in the shock tube are taken at the peak radiation point. In the computations, this is determined as the point of maximum radiative loss. The computed radiative emission at the peak radiation point is also presented in Fig. 6. The computed spectral emission qualitatively agrees with both experiments. The computed spectra, unlike experiments, show sharp atomic lines. This is due to spectral averaging in the experiment because of low spectral resolution. Quantitatively, the computed spectral emission lies below both of the experimental data. The computed lower emission is consistent with

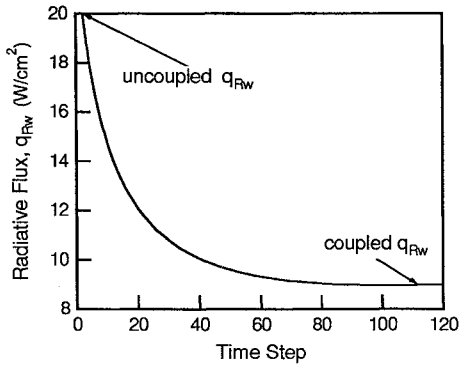

Fig. 2 Convergence of total radiative flux at the stagnation point.

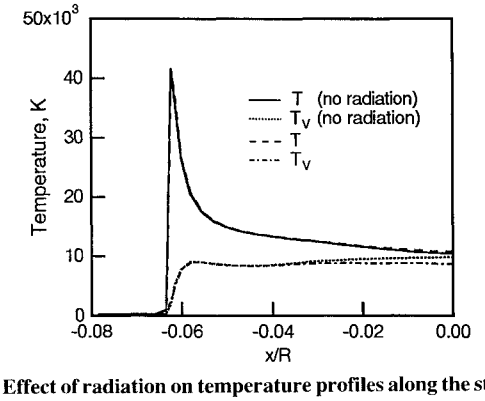

Fig. 3 Effect of radiation on temperature profiles along the stagnation streamline.

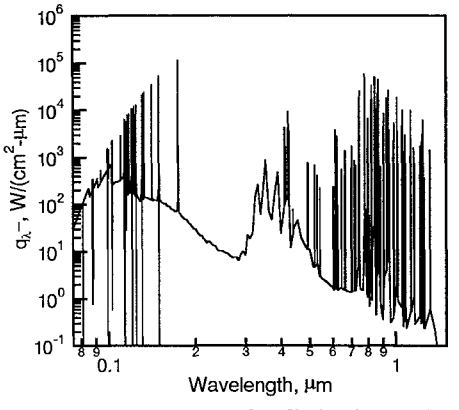

Fig. 4 Computed incoming spectral radiative flux at the stagnation point.

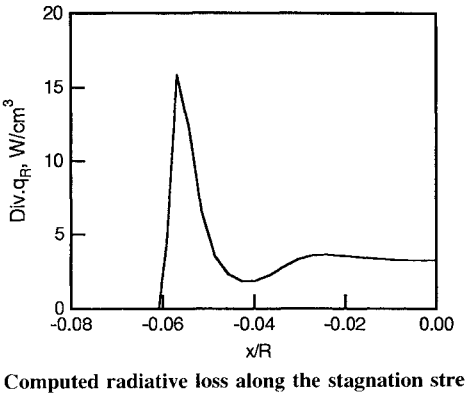

Fig. 5 Computed radiative loss along the stagnation streamline.

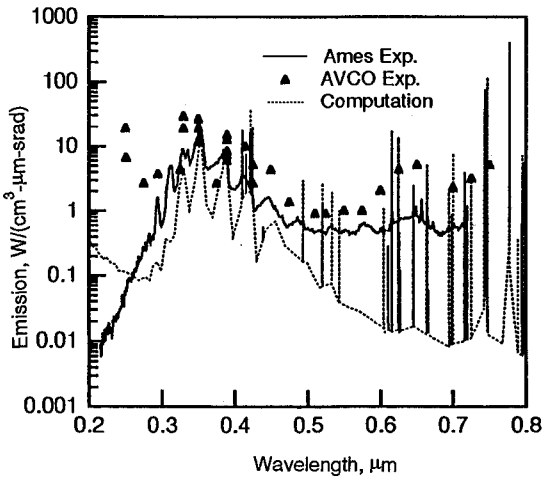

Fig. 6 Comparison of computed emission with the experimental data at the peak radiation point.

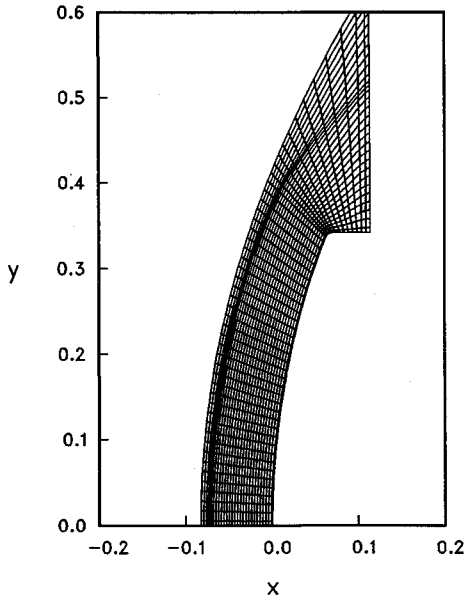

Fig. 7 Geometry of Fire II and computational grid (50 × 30).

the computed lower vibrational-electronic temperature at the peak radiation point. This comparison suggests a need for further investigation of the cause of low T_v. The present computations are primarily intended to demonstrate the capability of coupled detailed radiation simulations, therefore the assessment of the vibrational relaxation models is not attempted.

Fire II Flight Case

The conditions corresponding to the trajectory of Fire II flight at $t = 1634.25$ s are chosen for the computations. The freestream air at $u_\infty = 11.35$ km/s, $T_\infty = 191.6$ K, and $\rho_\infty = 4.265 \times 10^{-5}$ kg/m^3 are prescribed. Figure 7 depicts the Fire II geometry and computational adaptive grid of 50 × 30.

The computed spectral radiative fluxes at the stagnation point of Fire II, using coupled and uncoupled approaches, are presented in Fig. 8. The computations show the nongray nature of the radiating flowfield. Although the coupled spectral flux is lower than the uncoupled flux throughout the spectrum, the coupling effects strongly vary over the spectrum. Since the spectral flux expression involves integration along an optical path, the change in the spectral flux at the wall reflects the changes in overall flowfield. As the optical thickness of the gas varies in the wavelength, so does the effect of overall flowfield in the spectral flux.

In Fig. 9, the computed radiation intensity at the stagnation point is compared with the Fire II flight data.[15] The measurements cover the spectral range 0.2–0.6 μm. From Fig. 8, one sees that this portion of the spectrum is not significantly affected by the radiation coupling. The difference between the experimental data and the computations in the wavelength region below 0.35 μm is attributable to absorption of radiation by the quartz window used in the experiment at elevated temperatures. The computed intensity from the molecular bands qualitatively agrees with the flight data, but the absolute intensity from the atomic lines appears to be stronger than the experimental spectra show. This discrepancy is due to the smearing effect of radiation data gathering: the resolution of the radiometer is not sufficient to record the atomic lines accurately.

The computed total radiative fluxes along the Fire II surface and the stagnation streamline are presented in Figs. 10 and 11. In Fig. 10, the coupled and uncoupled computations are shown and are compared with the Fire II flight data measured by the radiometer at the stagnation point.[14] From Fig. 10, it is observed that the coupled radiative flux along the surface

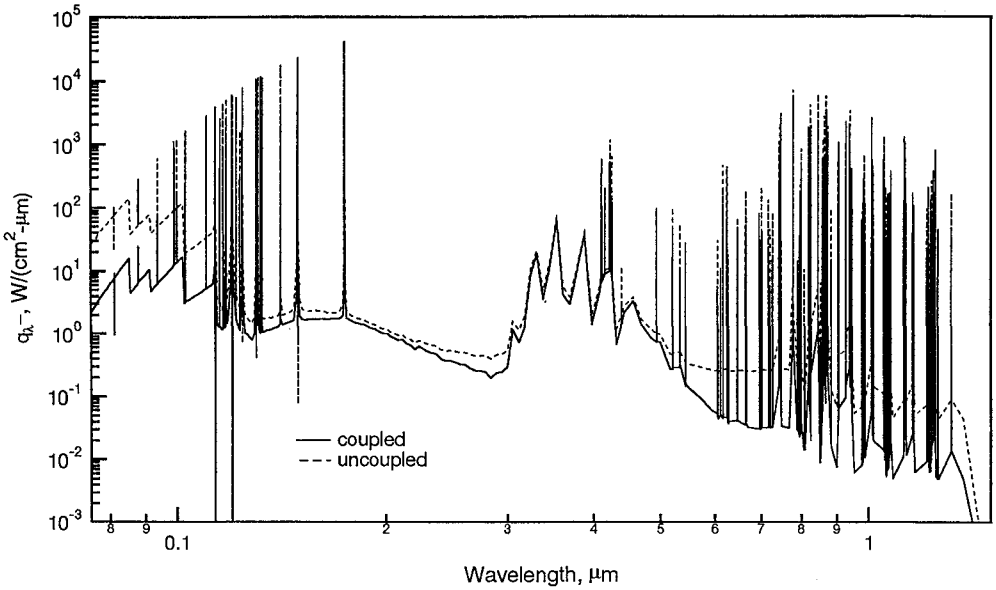

Fig. 8 Coupled and uncoupled computed spectral flux at the stagnation point of the Fire II vehicle.

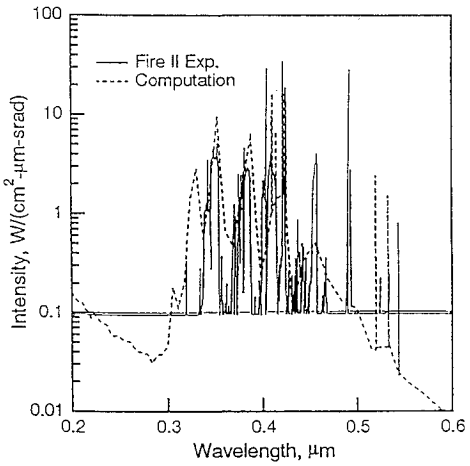

Fig. 9 Comparison of computed radiation intensity with the Fire II flight data at the stagnation point.

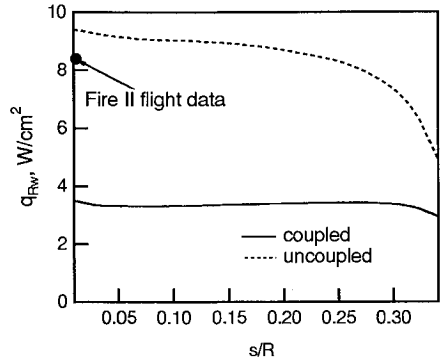

Fig. 10 Computed total radiative flux along the Fire II surface.

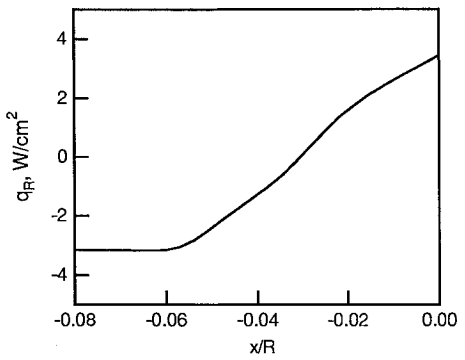

Fig. 11 Computed total radiative flux along the stagnation streamline.

is substantially lower than the uncoupled computations (by a factor up to 2.7), and the flight data lies between the coupled and uncoupled predictions. The fact that it is close to the uncoupled prediction is likely to be a coincidence. The low calculated values of radiative flux may also be attributed to the low peak vibrational-electronic temperature in the present computation. Note that small changes in vibrational-electronic temperature can translate into large differences in radiative flux predictions.

From the examination of Figs. 10 and 11, it is noted that the variation of the radiative flux along the surface is small compared with the variation along the stagnation streamline. This justifies the tangent-slab approximation used in the radiation modeling. In Fig. 11, the negative values of the flux represent the direction towards the freestream and positive values, the direction towards the wall. The total flux remains constant at the upstream of the shock since the gas is assumed to be transparent at the freestream.

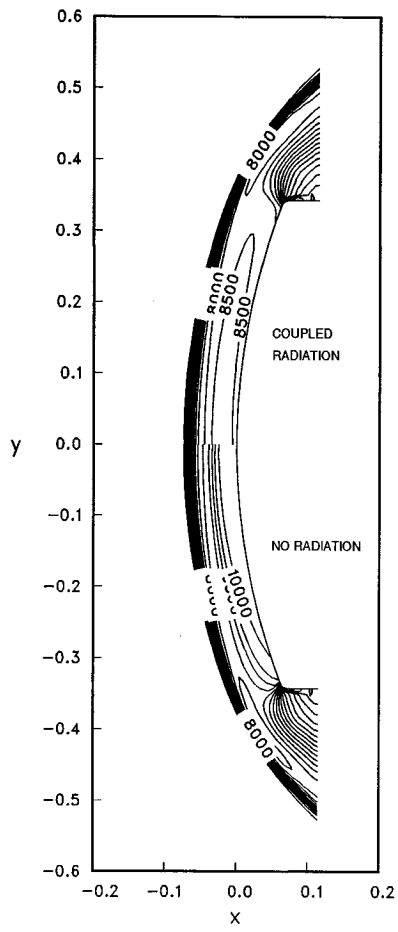

Fig. 12 Effect of radiation coupling on the flowfield contours of vibrational-electronic temperature over the Fire II vehicle.

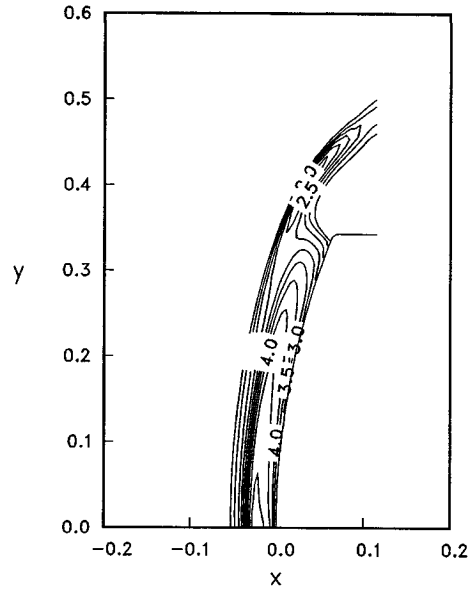

Fig. 13 Computed total radiative emission contours of the flowfield over the Fire II vehicle: W/cm³.

It has been observed that the vibrational-electronic temperature is the flowfield property most affected by radiation coupling. The effect of radiation on the vibrational-electronic temperature contours of flowfield is presented in Fig. 12. The vibrational-electronic temperature flowfield with coupled radiation shows nonadiabatic flow features near the wall due to radiative cooling. As seen from Fig. 12, the temperature de-

creases near the wall where radiation affects the flowfield most.

Finally, Fig. 13 shows the total radiative emission contours computed from the coupled flowfield solution. Total radiative emission is obtained by integrating the spectral emissivity over the wavelength range.

Concluding Remarks

A two-dimensional/axisymmetric thermochemical nonequilibrium code is developed for coupling radiative transfer with flowfield using tangent-slab approximation and a detailed spectral model. Fully coupled equations of flowfield and radiation are solved numerically using an implicit modified Gauss-Seidel line relaxation method. The numerical solutions of nonequilibrium flows with coupled radiation are presented for two test cases. For both cases, the computations and experimental data are in qualitative agreement. The calculation underestimates the total radiative flux reaching the surface, probably because of the low vibrational-electronic temperature obtained by the present model. The cause of the low temperature must be investigated. Also, the computations are currently inviscid; future work should include viscous and diffusion effects.

Acknowledgments

The author would like to acknowledge the support from NASA Ames Research Center Aerothermodynamics Branch through Grant Number NCC2-420. The author would also like to thank Chul Park for providing the curve-fits of absorption coefficients in the radiation model and for his helpful suggestions.

References

[1]Park, C., and Milos, F. S., "Computational Equations for Radiating and Ablating Shock Layers," AIAA Paper 90-0356, Jan. 1990.

[2]Gupta, R. N., Lee, K. P., Moss, J. N., and Sutton, K., "Viscous Shock-Layer Solutions with Coupled Radiation and Ablation for Earth Entry," *Journal of Spacecrafts and Rockets*, Vol. 29, No. 2, 1992, pp. 173–181; also AIAA Paper 90-1697, June 1990.

[3]Hartung, L. C., "Nonequilibrium Radiative Heating Prediction Method for Blunt Body Flowfields with Coupling to Flowfield Solvers," Ph.D. Dissertation, North Carolina State Univ. at Raleigh, Raleigh, NC, 1991.

[4]Carlson, L. A., and Gally, T. A., "Nonequilibrium Chemical and Radiation Coupling Phenomena in AOTV Flowfields," AIAA Paper 91-0569, Jan. 1991.

[5]Hartung, L. C., Mitcheltree, R. A., and Gnoffo, P. A., "Stagnation Point Nonequilibrium Radiative Heating and the Influence of Energy Exchange Models," AIAA Paper 91-0571, Jan. 1991.

[6]Hartung, L. C., "Development of a Nonequilibrium Radiative Heating Prediction Method for Coupled Flowfield Solutions," AIAA Paper 91-1406, June 1991.

[7]Gökçen, T., and Park, C., "The Coupling of Radiative Transfer to Quasi 1-D Flows with Thermochemical Nonequilibrium," AIAA Paper 91-0570, Jan. 1991.

[8]Hartung, L. C., and Hassan, H. A., "Radiation Transport Around Axisymmetric Blunt Body Vehicles Using a Modified Differential Approximation," AIAA Paper 92-0119, Jan. 1992.

[9]Cinnella, P., and Elbert, G. J., "Two-Dimensional Radiative Transfer Calculations for Flows in Thermo-Chemical Non-Equilibrium," AIAA Paper 92-0121, Jan. 1992.

[10]Hartung, L. C., Mitcheltree, R. A., and Gnoffo, P. A., "Coupled Radiation Effects in Thermochemical Nonequilibrium Shock Capturing Flowfield Calculations," AIAA Paper 92-2868, June 1992.

[11]Allen, R. A., Rose, P. H., and Camm, J. C., "Nonequilibrium and Equilibrium Radiation at Super-Satellite Reentry Velocities," AVCO-Everett Research Lab. Rept. 156, Sept. 1962.

[12]Sharma, S. P., Gillespie, W. D., and Meyer, S. A., "Shock Front Radiation Measurements in Air," AIAA Paper 91-0573, Jan. 1991.

[13]Cornette, E. S., "Forebody Temperatures and Calorimeter Heating Rates Measured During Project Fire II Reentry at 11.35 Kilometers per Second," NASA TM X-1305, Nov. 1966.

[14]Cauchon, D. L., "Radiative Heating Results from the Fire II Flight Experiments at a Reentry Velocity of 11.4 Kilometers per Second," NASA TM X-1402, July 1967.

[15]Cauchon, D. L., McKee, C. W., and Cornette, E. S., "Spectral Measurements of Gas-Cap Radiation During Project Fire Flight Experiments at Reentry Velocities near 11.4 Kilometers per Second," NASA TM X-1389, Oct. 1967.

[16]Whiting, E. E., and Park, C., "Radiative Heating at the Stagnation Point of AFE Vehicle," NASA TM-102829, Nov. 1990.

[17]Park, C., Howe, T. H., Jaffe, L. R., and Candler, G. V., "Chemical-Kinetic Problems of Future NASA Missions," AIAA Paper 91-0464, Jan. 1991.

[18]Park, C., *Nonequilibrium Hypersonic Aerothermodynamics*, Wiley, New York, 1989.

[19]Gnoffo, P. A., Gupta, R. N., and Shinn, J. L., "Conservation Equations and Physical Models for Hypersonic Air Flows in Thermal and Chemical Nonequilibrium," NASA TP-2867, Feb. 1989.

[20]Millikan, R. C., and White, D. R., "Systematics of Vibrational Relaxation," *Journal of Chemical Physics*, Vol. 39, No. 12, 1963, pp. 3209–3213.

[21]Boyd, I. D., and Gökçen, T., "Evaluation of Thermochemical Models for Particle and Continuum Simulations of Hypersonic Flow," AIAA Paper 92-2954, June 1992.

[22]Boyd, I. D., and Gökçen, T., "Computation of Axisymmetric and Ionized Flows Using Particle and Continuum Methods," AIAA Paper 93-0729, Jan. 1993.

[23]Park, C., private communication, NASA Ames Research Center, Moffett Field, CA, 1992.

[24]Park, C., "Nonequilibrium Air Radiation (NEQAIR) Program: User's Manual," NASA TM-86707, July 1985.

[25]Abramowitz, M., and Stegun, I. A., *Handbook of Mathematical Functions*, Dover, New York, 1972, pp. 228–237.

[26]MacCormack, R. W., "Current Status of the Numerical Solutions of the Navier-Stokes Equations," AIAA Paper 85-0032, Jan. 1985.

[27]Candler, G. V., "The Computation of Weakly Ionized Hypersonic Flows in Thermo-Chemical Nonequilibrium," Ph.D. Dissertation, Stanford Univ., Stanford, CA, 1988.

[28]Gökçen, T., "Computation of Hypersonic Low Density Flows with Thermochemical Nonequilibrium," Ph.D. Dissertation, Stanford Univ., Stanford, CA, 1989.